Impact of experimental effects on a resolved resonance evaluation for practical applications

L. Leal, Nicolas Leclaire, Jaiswal Vaibhav

Annals of Nuclear Energy 208 (2024) 110795

Contents lists available at ScienceDirect

Annals of Nuclear Energy

journal homepage: www.elsevier.com/locate/anucene

Impact of experimental effects on a resolved resonance evaluation for practical applications☆

L. Leal [a,*], N. Leclaire [b], V. Jaiswal [b]

[a] Oak Ridge National Laboratory, Nuclear Energy and Fuel Cycle Division, Oak Ridge, TN, 37831, United States of America
[b] Institut de Radioprotection et de Sûreté Nucléaire, 31 avenue de la division Leclerc, Fontenay-aux-Roses, 92260, France

ARTICLE INFO

Keywords:
Nuclear data
Low temperature
Differential and integral data
Data evaluation

ABSTRACT

Nuclear data evaluations available in existing nuclear data libraries are derived based on differential measurements that includes experimental effects such as target temperature, time-of-flight resolution, data normalization, self-shielding, multiple scattering, etc. Measurements are often made at temperatures corresponding to room temperature, 293.6 K, to avoid complexity in the experimental setup and costs of carrying out measurements for temperatures other than room temperature. This paper investigates the impact of experimental effects on the evaluation of a set of resonance parameters that fit the experimental differential data and its use in integral benchmark calculations. Given the importance of the temperature in integral benchmark results, the impact of the Doppler effect will be examined. Very seldom are experimental differential data available for temperatures below or above room temperature. Nuclear data measurements and evaluation needs are driven by reactor applications; consequently, the majority of data evaluations in nuclear data libraries are for temperatures above room temperature. Recently there has been a demand for nuclear data for low temperatures, below room temperatures, for criticality safety applications. Currently, calculations in response to low-temperature needs are based on extrapolating the existing data from the nuclear data libraries to temperatures below 293.6 K. For temperatures above 293.6 K, common practice is to process the data library to temperatures different from the temperature it was evaluated and use them in practical applications. Although this is an acceptable practice, care should be taken to understand whether the validity of the nuclear data can be extended to low and high temperatures. Issues in connection with temperature effects for low and high temperature nuclear data and their impact on practical applications are addressed in the paper. Given that experimental data for low- and high-temperatures are scarce, the results of the presented approach are based on data simulations. Simulated data for ^{235}U in the resonance region, in particular the resolved resonance region, were used as part of the studies and demonstration. Furthermore, temperature effects were also investigated for thermal neutron scattering data, $S(\alpha, \beta)$, for light water. However, the thermal scattering data are not based on simulation, but are the result of measurements carried out at the Spallation Neutron Source. A continuous-energy nuclear data library was used in Monte Carlo calculations to assess the impact in integral benchmark results.

1. Introduction

Energy-dependent nuclear cross-section data measurements, often referred to as differential data, are carried out at experimental facilities throughout the world and are collected for inclusion in nuclear data repositories such as the EXFOR experimental database Otuka et al. (2014). Time-of-flight (TOF) experiments using linear accelerators as pulsed neutron sources are being conducted at nuclear cross-section measurement facilities such as the Gaerttner Linear Accelerator (Gaerttner and M. L. Yeater, 1961) at the Rensselaer Polytechnic Institute in the United States, the Spallation Neutron Source (SNS) (The Spallation Neutron Source (SNS)) at Oak Ridge National Laboratory (ORNL) in

* Corresponding author.
E-mail address: leallc@ornl.gov (L. Leal).

https://doi.org/10.1016/j.anucene.2024.110795
Received 7 May 2024; Received in revised form 11 July 2024; Accepted 15 July 2024
Available online 24 July 2024

the United States, the Geel Electron Linear Accelerator (GELINA) (Bensussan and Salome, 1978) in Belgium, and the n_TOF machine at the European Organization for Nuclear Research (CERN) (Rubbia et al., 1998) in Geneva, Switzerland. Note that for the same measured data, for instance the captured cross-section measurement done at different measurement facilities, the energy-dependent measured data values will likely be distinct because of the experimental conditions. For instance, target temperature, TOF resolution, data normalization, self-shielding, and multiple scattering effects are some examples of quantities that define the experimental conditions. For a reaction x, the experimental effective cross section, namely, $\langle\sigma_x(E)\rangle$, which relates to the true cross-section $\sigma_x(E)$, is given as

$$\langle\sigma_x(E,\Delta)\rangle = \int f(E,E',\Delta)\,\sigma_x(E')dE', \tag{1}$$

where the function $f(E,E',\Delta)$ describes the experimental conditions (temperature effects, TOF resolution, etc.). The function $f(E,E',\Delta)$ is a convolution of functions that describe the experimental effects. The work of the nuclear data evaluator is to understand the details of the experimental effects to get the best estimation of the true cross-section $\sigma_x(E)$. Nuclear data evaluation tools exist (Larson, 2008) that permit evaluators to mock up the experimental effects. Note that for practical applications such as reactor design and calculation, criticality safety analysis, and so on, it is the effective cross section, that is, the evaluated cross-section $\langle\sigma_x(E,\Delta)\rangle$ that will be Doppler broadened to account for the temperature effect. The usual procedure consists of a convolution of the evaluated cross section, with a function (kernel) that includes the temperature effects in a form similar to Eq. (1). Solbrig's Kernel (Solbrig, 1961) is frequently used for the Doppler broadening of the cross section. Clearly, the closer $\langle\sigma(E,\Delta)\rangle$ is to $\sigma_x(E)$ the better the results of practical application will be.

The most common practices for data measurements have been to use the target sample at room temperature, that is, 293.6 K. Undoubtedly, most of the experimental data available in the nuclear data repository are for room temperatures. Consequently, the evaluations in the nuclear data libraries can be, at best, trusted for the temperature for which the data were evaluated. In this paper, an investigation on the applicability of nuclear data for temperatures different from those for which they were evaluated is performed. The effect of the low- and high-temperature, cross-section data was investigated for application on benchmark systems including ^{235}U and the light water thermal scattering kernel $S(\alpha,\beta)$. Simulated cross-section data were generated for ^{235}U whereas for the light-water $S(\alpha,\beta)$ frequency spectrum from low-temperature measurements carried out at SNS (The Spallation Neutron Source (SNS)) were used. Low-temperature data needs have gained interest since emergence of the International Atomic Energy Agency (IAEA) transport regulatory requirements related to the safety of the criticality of nuclear material transportation IAEA (2018). The IAEA nuclear data temperature requirements for package transportation of nuclear material are clearly defined in the range from −40 C (233.15 K) and above.

This paper is organized as follows. Section 2 describes the approach used to simulate the experimental data through the resonance parameter generation using known resolution function and experimental effects. The resonance parameters obtained by fitting the simulated experimental data are presented. Comparisons are made of the results of calculations done with the resonance parameters used to simulate the experimental and the parameter set obtained by fitting the simulated data. The temperature effects on the cross section are investigated. Section 3 presents the temperature effects at low energy based on thermal neutron scattering. The temperatures range from below room temperature (293.6 K), as low as 6 K, to high temperatures, as high as 550 K. The effect of the phonon spectrum for these temperatures is considered. The impact of using the temperature effects on practical applications for temperatures below and above room temperature is presented in Section 4. Conclusions from the research are presented in Section 5.

Table 1
Average ^{235}U resonance parameters.

	$J^\pi = 3^-$	$J^\pi = 4^-$
Energy level spacing (eV)	1.13(7)	0.83(4)
s-wave strength function (10^{-4})	0.84(5)	0.96(5)
Fission width (meV)	269.3(518)	158.2(158)
Gamma capture width (meV)	40.0(9)	39.5(8)

2. Methodology description

2.1. Resonance parameter generation

As temperature, the so-called Doppler effect, impacts the cross section in the resonance region (RR), the basic approach was to simulate the cross sections in this energy region. ^{235}U like isotope cross-section data were simulated in the energy region from 10^{-5} eV to 2.25 keV. The energy range is similar to that of the resolved resonance region of the actual ^{235}U evaluation in the evaluated nuclear data libraries Leal et al. (2017). The steps used in the simulated data generation consisted of generating resolved resonance parameters as follows:

(a) Use actual ^{235}U average resonance parameters for generating pseudo resonance parameters. The average parameters are those listed in Table V of Leal et al. (2017) and are shown in Table 1.

(b) Sample resonance parameters based on the usual Wigner and Porter-Thomas distribution laws, for energy level spacing and widths, respectively.

The spacing between two consecutive resonance energies for the same total angular momentum and parity, $D_\lambda = E_{\lambda+1} - E_\lambda$, follows the probability distribution function predicted by Wigner's law Leal and Larson (1995). If the average level spacing is $\langle D\rangle$ the probability distribution function is,

$$p(x)dx = \frac{\pi x}{2} exp(-\frac{\pi x^2}{4})dx\ , \tag{2}$$

where $x = D_\lambda/\langle D\rangle$.

Resonance widths, Γ_λ, show fluctuations between resonances of the same angular momentum and parity. The probability distribution function for the widths Γ_λ is a χ^2 distribution with ν degrees of freedom given as

$$p(x)dx = \frac{\nu}{2G(\nu/2)}(\frac{\nu x}{2})^{\frac{\nu}{2}-1} exp(-\frac{\nu x}{2})dx\ , \tag{3}$$

where $x = \Gamma_\lambda/\langle\Gamma\rangle$ and $G(\nu/2)$ is the mathematical gamma function and $\langle\Gamma\rangle$ is the average value of the resonance width taken over a given energy range. In particular, for $\nu = 1$, Eq. (3) is known as the Porter-Thomas distribution law for the reduced neutron width. Two fission channels were used, and the sampling for the fission widths for the two spins were done with a degree of freedom $\nu = 2$.

The spin of the resonances was sampled by assuming a level spacing density proportional to $2J + 1$. Evidently, according to Table 1, many more resonances are found for $J^\pi = 4^-$ in comparison with the $J^\pi = 3^-$ resonance spin state.

Only s-wave resonances are simulated. A resonance parameter set of about 4727 s-wave resonances, for which 2132 are for $J^\pi = 3^-$ and 2595 for $J^\pi = 4^-$, respectively, in the energy region up to 2.25 keV were generated with the information listed in Table 1. It is believed that the sampled resonance parameters are complete in the sense that no resonance is missing. The resonance parameters were converted into the SAMMY format (Larson, 2008). The Reich–Moore approach was used to generate the cross sections. The resonance parameters needed for the Reich–Moore calculations of a fissile isotope are the resonance energy E_r, the gamma width Γ_γ, neutron width Γ_n, two fission widths Γ_{f1} and Γ_{f2}, respectively, and the spin and parity J^π.

Table 2
Data information (T = 293.6 K).

	Energy range (eV)	Flight path and density
Transmission		
TData1 (Spencer et al., 1987)	0.01–8.0	L = 18 m, n = 0.00147 atom/barn
TData2 (Harvey et al., 1988)	0.4–100	L = 18 m, n = 0.03269 atom/barn
TData3 (Harvey et al., 1988)	100–2250	L = 80 m; n = 0.03269 atom/barn
Fission		
FData1 (Gwin et al., 1984)	0.01–20.0	L = 25.6 m
FData2 (Weston and Todd, 1984)	14–500	L = 18 m
FData3 (Weston and Todd, 1984)	100–2500	L = 85.5 m
Capture		
CData1 (Perez et al., 1973)	0.01–2250	L = 85.5 m

2.2. Cross-section data generation

Some essential steps are needed to simulate the experimental data from the resonance parameters previously derived in the energy region 10^{-5} eV to 2.25 keV. Energy mesh, resolution function, and temperature were chosen according to information provided for existing measured data. The simulation of experimental data will provide relevant information for the proposed study and for understanding the effect of temperature. The information provided in Table 2, equivalent to that of Leal et al. (2017), was used to generate transmission data (total cross section), fission cross section, and capture cross section. The Spencer et al. (1987) and Harvey et al. (1988) information was used to generate transmission data. The Gwin et al. (1984) and Weston and Todd (1984) information was used to generate the fission data, and the capture data were generated on the basis of Perez et al. (1973) Table 2 shows the details of what was used to simulate the experimental data. As an example, the resolution function of the transmission data of Harvey et al. resembling a Gaussian and exponential tail folding, is shown in Fig. 1, which would correspond to the function $f(E, E', \Delta)$ in Eq. (1).

The further step in the simulation consisted of adding random Gaussian noise to the data. This is a standard, reasonable way of adding noise to data. Uncertainties in the simulated data were added according to the actual data uncertainties for the data listed in Table 2. The fission, capture, and scattering simulated data were normalized at thermal to the ^{235}U standard cross-section values, which are 586.4(15) barns, 99.1(21) barns, and 14.03(22) barns, respectively. All the data were generated at room temperature, that is, T=293.6 K. The simulated data were generated with the SAMMY code based on the resonance parameters derived in the previous section. The simulated data for the total, fission, and capture cross sections are shown in Fig. 2 in the energy range of 100 to 150 eV. As a matter of visual comparison, the actual fission cross section of Weston and Todd (1984) and that simulated and identified in Table 2 as FData3, is shown in Fig. 3 in the energy range of 100 to 150 eV.

Note that the pseudo set of resonance parameters will be referred to as the full_set. The cross sections calculated using the full_set will serve as the reference values for comparisons. Further, the simulated data will be the "experimental" data. For the fitting process of the simulated data, it is assumed that no information on the full_set is available. The only available information is that regarding the simulated data: their energy dependence and the related resolutions.

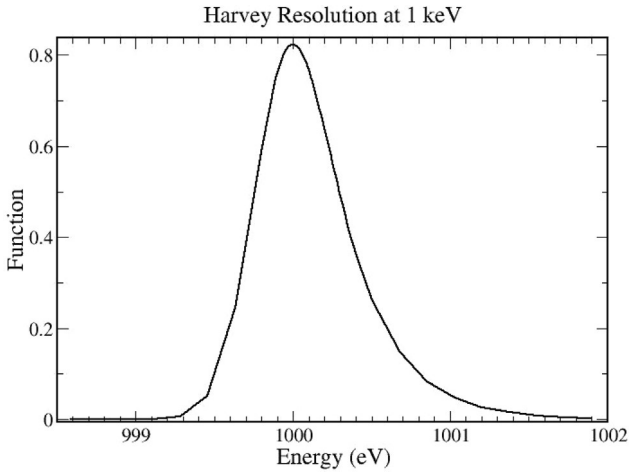

Fig. 1. Transmission resolution at 1 keV.

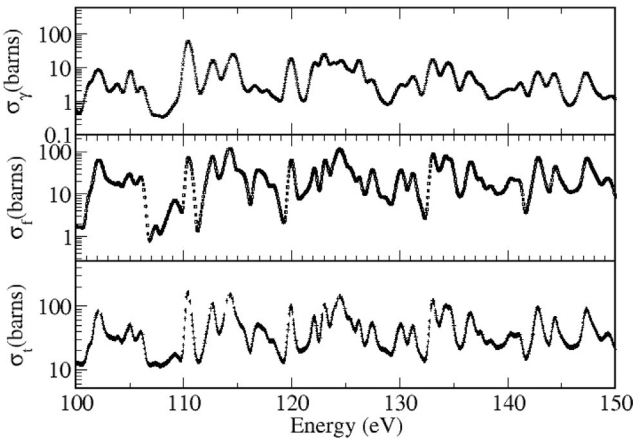

Fig. 2. Total, fission, and capture simulated data ^{235}U.

2.3. Simulated data fitting

The simulated data shown in Table 2 serves as the experimental data for the fitting in the energy region up to 2.25 keV. The approach consists of searching, from scratch, resonance parameters that fit, simultaneously, the simulated total, fission, and capture cross-section data. The fitting is carried out with the SAMMY code. At a minimum, SAMMY requires three inputs: (1) the experimental data, which in this case are the simulated data; (2) an input including information on the spin, scattering radius, resolution, etc.; and (3) the set of resonance parameters that are used to fit the data. Evidently, the challenge is to find the resonance parameters that fit the experimental data (simulated data). Again, it is assumed that no knowledge exists regarding the full_set. The usual procedure for fitting actual experimental data was used here, and resonance parameters were identified that fit simultaneous and reasonably well, the simulated data. The intent is not to explain the details of how the fit was performed since explanations can be found elsewhere Leal et al. (1999). The fittings were carried out for the simulated data at a temperature of T = 293.6 K.

A set of resonance parameters containing about 3370 resonances (1546 for the spin $J = 3^-$ and 1824 for $J = 4^-$) was derived in the evaluation. The set represents a shortage of about 40% less

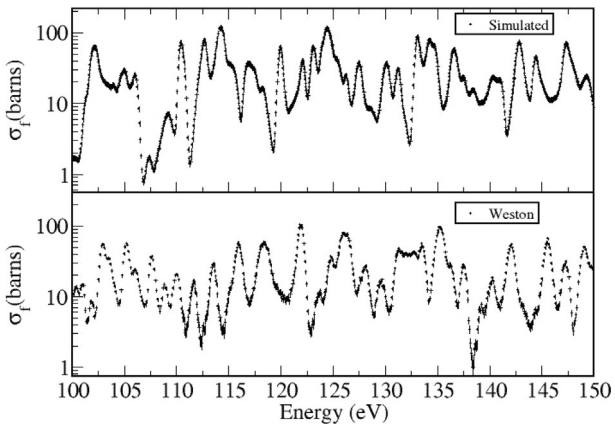

Fig. 3. Weston fission cross section and simulated data for ^{235}U.

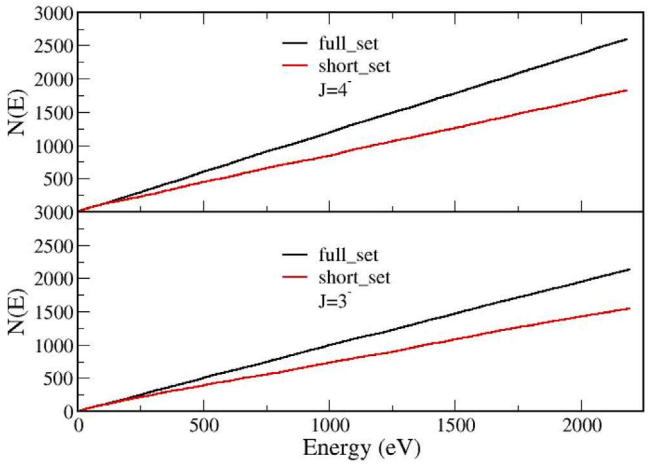

Fig. 4. Cumulative number of energy levels.

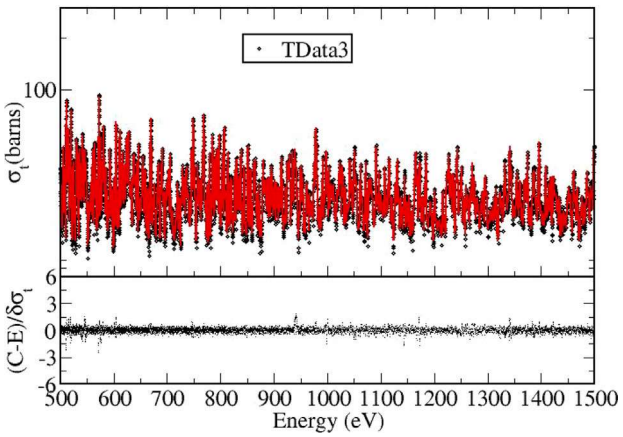

Fig. 5. Total cross-section fitting.

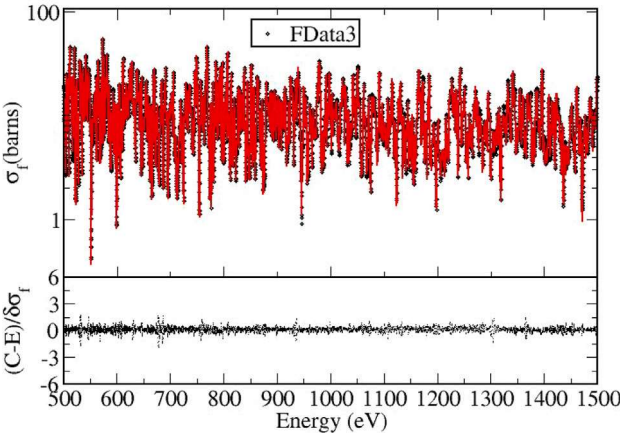

Fig. 6. Fission cross-section fitting.

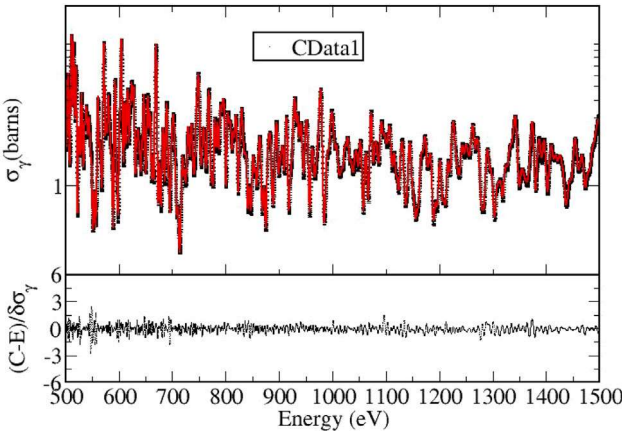

Fig. 7. Capture cross-section fitting.

resonances in comparison with the full_set (4724 resonances). The number of energy levels as a function of the energy is shown in Fig. 4, which clearly demonstrates the number of missing resonances for each resonance spin J. We refer to the reduced set of resonance parameters as the short_set. As will be seen, the number of missing resonances will show some impact in the extrapolation of the resonances derived in the evaluation at $T = 293.6$ K to lower and higher temperatures. The quality of fitting for the total, fission, and capture cross sections, which correspond to TData3, FData3, and Cdata1 in Table 2, respectively, are shown in Figs. 5, 6, and 7, respectively, in the energy range from 500 eV to 1.5 keV, as well as the corresponding residues. In the next section, cross-section calculations with both resonance parameters – short_set and full_set – are carried out to demonstrate the data temperature issue.

2.4. Tests and calculations with the resonance parameters full_set and short_set

Results of calculations using the resonance parameter short_set for several temperatures are compared with the results using the resonance parameter full_set, which is taken as the references. Both the full_set and the short_set were converted into the ENDF (END, 2010) resonance parameter format using the LRF=7 option. The JEFF-3.3 ^{235}U evaluation was used as the template, and the ENDF-formatted resolved resonance parameters replaced the existing JEFF-3.3. The libraries are referred to hereafter as JEFF-3.3_FULL and JEFF-3.3_SHORT. It should be noted that only the part corresponding to the ^{235}U resolved resonance region was replaced in the JEFF-3.3 evaluation for both JEFF-3.3_SHORT and JEFF-3.3_FULL and everything else is entirely from the JEFF-3.3 library. Temperature-dependent cross sections were calculated with the NJOY (Macfarlane et al., 2017) code for several temperatures using the usual RECONR and BROADR schemes. The NJOY results at room temperature for the thermal fission, capture, and scattering cross sections (i.e., σ_f, σ_γ, and σ_s), respectively, are shown in Table 3. The thermal cross section values are about the same as those listed in the International Atomic Energy Commission (IAEA) nuclear data standards of 2018 (Carlson et al., 2018). The

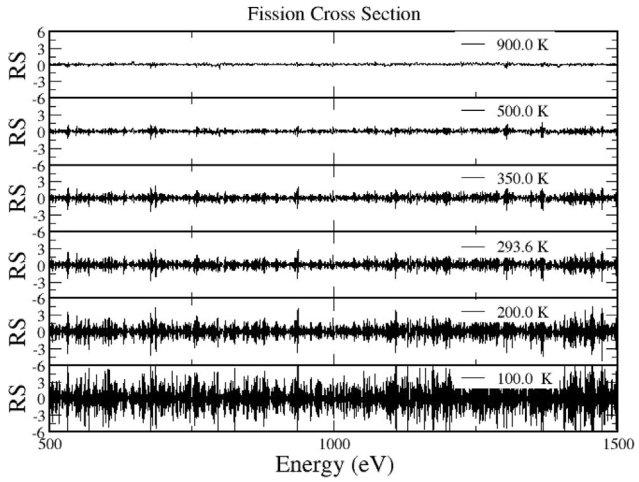

Fig. 8. Fission cross-section residues.

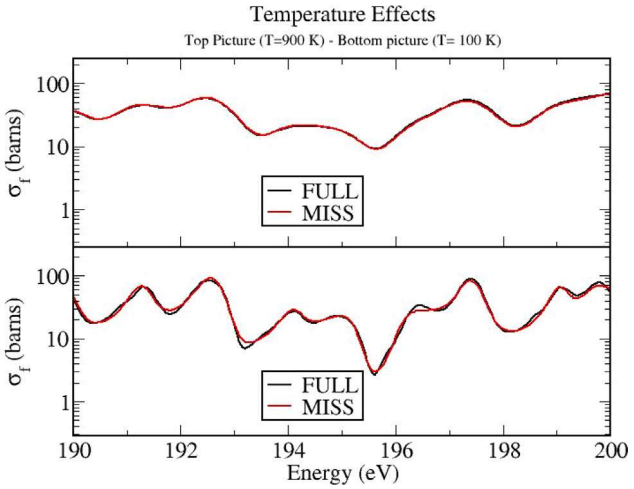

Fig. 9. Fission cross section for temperatures 100 K and 900 K.

resonance capture (I_γ) and fission (I_f) integrals are also displayed in Table 3. As can be seen from Table 3, the results of the short resonance parameter reproduce well the values corresponding to the full parameters. The further steps consist of comparing the calculated point cross sections for different temperatures. To do this, the residuals defined as the difference between the cross sections calculated with the full resonance parameters minus the cross sections calculated with the short resonance parameter divided by the uncertainty of the data are compared. Although the data uncertainty is for the room temperature, it is assumed that they do not change much for other temperatures. This assumption does not seem to hinder demonstration of the proposed approach.

The calculated residues for the fission cross sections, indicated as RS which is defined as $(C-E)/\delta\sigma_f$, for the temperatures 100 K, 200 K, 293.6 K, 350 K, 500 K, and 900 K, respectively, in the energy range 500 eV to 1.5 keV, are shown in Fig. 8. From the viewpoint of the differential data, interesting patterns are observed:

(a) The residues corresponding to the temperature 293.6 K are equivalent to that of Fig. 6 except that in the residues of Fig. 6 the calculated cross section includes the data resolution.

(b) Taking the room temperature (293.6 K) as the reference, it is noted that an increase in the temperature leads to a decrease in the residues; on the contrary, for lower temperatures, the residues increase. This is expected because the temperature Doppler effects cause the resonances to be less pronounced as the temperature increases. This can be seen from Fig. 9. The calculated fission cross section for the short and full resonance parameters are shown for the temperatures 100 K (bottom) and 900 K (top) in the energy region from 190 to 200 eV. The cross-section difference for the high temperature (900 K) is negligible, whereas for the low temperature (100 K), it is clearly visible. Listed in Table 4 are the χ^2 corresponding to the fission cross section for the five temperatures. The χ^2 was normalized to the value of the temperature 293.6 K. The lower value for χ^2 indicates small cross-section differences between calculations with the short and full resonance parameter sets.

(c) Apparently, the residues for the temperatures 200 K and 293.6 K are not too different. This could indicate that the short set of resonance parameters could provide results similar to that of the full set.

The actual impact of the short and full resonance sets in practical applications will be investigated using benchmark systems with the neutron spectrum in the thermal and intermediate energy regions.

Table 3
^{235}U thermal and resonance integral.

Values	JEFF-3.3_FULL (eV)	JEFF-3.3_SHORT (eV)
σ_f	584.1	584.1
σ_γ	99.1	99.1
σ_s	14.4	14.4
I_γ	145.4	145.2
I_f	633.1	634.8

Table 4
Normalized χ^2 for five temperatures.

T(K)	χ^2
100.0	3.1
200.0	1.7
293.6	1.0
350.0	0.8
900.0	0.4

3. Impact of temperature on thermal scattering cross sections

The temperature impact on the cross sections has been investigated in previous sections for energies where the free gas approximation is valid. However, when the energy of the incident particle is comparable with the energy associated with the molecular thermal motion because of temperature effects, the free gas approximation can no longer be applied. More sophisticated approaches are needed to explain the effects of temperature, and the derived thermal scattering cross sections – often called the Thermal Scattering Laws (TSLs) – are the most appropriate quantities used in benchmark calculations. TSLs for a wide variety of moderating materials exist primarily for cross sections in the energy range of less than about 10 eV. More detailed description about the thermal scattering process can be found in the literature (Hove, 1954; MacFarlane, 1994; Mattes and Keinert, 2005; Marquez Damian et al., 2014). Using the first Born approximation and Fermi pseudo-potential, as formalized by Van Hove (Hove, 1954), the double-differential scattering cross-section (DDXS) for thermal neutrons with an incident energy E, scattering angle θ, scattered with final energy E', and at temperature T can be expressed as a function of $S(\alpha,\beta)$, by

$$\frac{d^2\sigma}{d\Omega dE'}\left(E\rightarrow E',\mu,T\right)=\frac{\sigma_b}{4\pi k_B T}\sqrt{\frac{E'}{E}}\,S(\alpha,\beta)\,, \tag{4}$$

where α represents the momentum change and β represents the change in energy.

$$\alpha=\frac{E+E'-2\mu\sqrt{EE'}}{Ak_BT},\qquad \beta=\frac{E'-E}{k_BT},\quad \text{and}\quad \sigma_b=\sigma_{free}\left(\frac{A+1}{A}\right)^2. \tag{5}$$

Here, A denotes the ratio of the scatterer mass to that of the neutron mass, σ_b the bound atom scattering cross section, σ_{free} the free atom scattering cross section, μ the cosine of the scattering angle, and k_B the Boltzmann constant. Under the incoherent and the Gaussian approximation, the TSL can be expressed as a function of the frequency spectrum $\rho(\beta)$ of the excitations in the molecular system by MacFarlane (1994):

$$S(\alpha,\beta) = \frac{1}{2\pi}\int_{-\infty}^{+\infty} e^{\iota\beta\hat{t}}\, e^{-\gamma(\hat{t})} d\hat{t}\ , \tag{6}$$

where t is the time measured in the units of $\hbar/(kT)$ seconds. $\gamma(\hat{t})$ is given by

$$\gamma(\hat{t}) = \alpha\int_{-\infty}^{+\infty} P(\beta)(1 - e^{-\iota\beta\hat{t}})\, e^{-\beta/2} d\beta\ , \tag{7}$$

and

$$P(\beta) = \frac{\rho(\beta)}{2\beta\sinh(\beta/2)}\ , \tag{8}$$

where $\rho(\beta)$ is the frequency spectrum of the interacting molecule.

Efforts are underway to better understand the impact of temperature on the thermal scattering cross sections of various moderators. In particular, several studies have been carried out, both on the simulation side using molecular dynamics simulations and using TOF experiments to generate thermal scattering evaluations. To better understand the impact of temperature on the TSLs, an example of light water TSLs are presented in the following section. The objective of this section is not to present a new evaluation but to introduce the complexities behind these kind of studies and to highlight the physics dealing with low-temperature TSLs. To achieve this goal, two TOF experiments with light water were carried out at SNS. The first set of experiments was carried out for room-temperature and high-temperature close to reactor operating conditions, and the other set was carried out for very low temperatures, all the way down from room temperature to 6 K.

TSL for Ice-*Ih* (a particular form of light water ice) and TSL for room temperature based on these measurements are introduced in the following section.

3.1. Below room-temperature cross sections

Interest is rising in the dynamics of the low-temperature light water cross sections, in particular Ice-*Ih*. The low-energy and low-temperature effects are important not only for fundamental physics and chemistry but also for nuclear reactor spent fuel applications. The dynamics of Ice-*Ih* can influence calculations for the design and development of shipping casks, fuel storage, reprocessing facilities, and criticality safety studies. Active research is underway on advanced nuclear systems using Ice-*Ih* as a neutron moderator (operating at about 80 K). Institutions such as the IAEA, UK Atomic Energy Authority, and the Institut de Radioprotection et de Sûreté Nucléaire (IRSN) have emphasized the need for Ice-*Ih* neutron scattering data in the temperature range of about 253–293 K.

Double-differential scattering cross-section and total cross-section measurements for Ice-*Ih* were conducted at the SNS SEQUOIA instrument Jaiswal et al. (2023). The experiments were carried out for different incident neutron energies (E_i = 11, 55, 160, 250, and 600 meV) and temperatures (T = 6, 100, 200, 233, 243, 253, 263, and 271 K). These measurements are an excellent investigative tool for probing the dynamical structure and physics of light water below room temperatures. Computational methods using material and physics models are the convention for TSL evaluations. However, double-differential scattering measurements constitute a powerful basis for validating theoretically produced S(α,β). These experiments also help identify and resolve biases or limitations in theoretical models and help in understanding the observed discrepancies between theoretically generated S(α,β) to those based on experimentally measured data. New thermal scattering libraries for light water ice based on SNS experiments and atomistic simulations are under development at IRSN. For completeness, the phonon spectrum obtained at various temperatures and 160 meV incident neutron energy is presented in Fig. 10. These high-resolution double-differential experiments help in obtaining the phonon spectra for the other experimental temperatures. The experimental data, along with atomistic simulations on ice, are still being processed at IRSN, and a new set of TSL evaluations for a series of temperatures is under development.

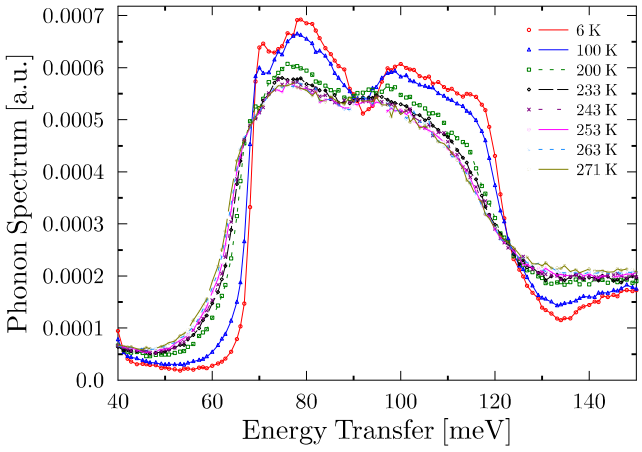

Fig. 10. Phonon spectrum of ice for incident neutron energy E_i= 160 meV.

Table 5
Thermodynamic conditions of the measurements for light water.

Temperature (K)	Pressure (bar)	Incident neutron energy (meV)
295	1	60, 160, 280, 800
323	1	60, 160, 280, 800
350	1	12, 60, 160, 280, 800
350	150	8, 60, 160, 280, 800
400	150	8, 60, 160, 280, 800
450	150	8, 60, 160, 280, 800
500	150	8, 60, 160, 280, 800
550	150	8, 60, 160, 280, 800

3.2. Room-temperature and high-temperature (Reactor conditions) cross sections

The need for accurate room-temperature cross sections and beyond (similar to reactor operating temperatures) has evolved in the past few years to precisely calculate reactor physics and criticality safety applications. Various research groups have dealt with accurate measurements of high-resolution double-differential data and data evaluation while also incorporating results from modern atomistic simulation. Recent efforts in advancing the cross sections based on atomistic simulations and the implementation of improved diffusion models have improved the cross section at room temperature significantly. Various experiments carried out at the Institut Laue-Langevin (ILL) and SNS highlighted complexities in the modeling of high-temperature cross sections. Further research is underway to develop improved thermal scattering cross sections for liquid light water both for room temperatures and beyond room temperatures based on recent experiments carried out at SNS and using molecular dynamics simulation. Double-differential scattering cross-section measurements were carried out at SNS for a series of temperatures and pressures. The objective was to obtain the phonon spectrum to be able to generate new improved TSL data from experimental data. Also, the double-differential data would serve as a benchmark to validate the developed evaluation. Table 5 shows the experimental conditions at which the experiments were carried out with light water in the liquid phase. As for the case of light

Table 6
Density (g/cm^3) of ICE/water as a function of temperature.

Values	115 K	233 K	293.6 K	600 K
ICE	0.9228	0.9228	–	–
Water	–	–	0.998	0.694

water ice, phonon spectra of liquid water at 295 K and for 160 meV incident neutron energy is presented in Fig. 11. The rotation band can be clearly observed in the phonon spectrum, the accurate knowledge of which is deemed necessary to generate reliable TSLs for light water. Development of TSLs for liquid light water is under development not only for room temperatures but also for reactor temperature and pressure conditions. Nevertheless, the objective of this section is to highlight the impact of temperatures on the thermal scattering data and, in particular, how when going below room temperature the results are significantly different. For instance, this effect can be seen by comparing the phonon spectrum of light water presented in Figs. 10 and 11. This difference in how neutrons exchange energies with different phonon modes of the scattering molecule at different temperatures will be well reflected in the benchmark studies.

4. Benchmark results

The impact of temperature effects on differential data is investigated in the preceding sections to some extent for temperatures below and above room temperature, that is 293.6 K. Although the previous sections provide useful information, the impact of temperature effects on practical applications is necessary. This can be achieved by using the simulated data previously derived in integral benchmark calculations. To test the impact of the simulated libraries, JEFF-33_FULL and JEFF-33_SHORT for ^{235}U, two sets of benchmarks were used: (1) the OECD/WPNCS/SG3 benchmark (Cabellos and Piedra, 2018) featuring a pressurized water reactor (PWR) 17 × 17 assembly with 25 guide tubes filled with water at various burnups and (2) a theoretical benchmark involving an infinite fissile medium with fixed concentrations of ^{235}U and a varying content of water to cover a wide range of neutron energies.

The libraries, JEFF-33_FULL and JEFF-33_SHORT for ^{235}U, were processed for four temperatures: 115 K, 233 K, 293.6 K, and 600 K using the 2016.75 release of the NJOY code Macfarlane et al. (2017). The thermal scattering data were also generated at the temperatures 115 K, 233 K, and 293.6 K. Anything else in the benchmark was taken from the JEFF-3.3 library.

Multiplication factor, k_{eff}, calculations were carried out with the Monte Carlo MORET 5 code (Cochet et al., 2015) using a continuous energy description of the nuclear data. The targeted Monte Carlo standard deviation was set lower than 20 pcm.

For the first benchmark, only the zero burnup configuration was considered. The fuel was fresh UO_2 with uranium enriched at 4.5 wt percent in ^{235}U. The 264 fuel rods were set in a lattice at a 1.265 cm square pitch. The pellet radius was 0.412 cm, and the outer clad radius 0.476 cm. The assembly was surrounded by 1 m of ice or water, depending on the temperature. Four temperatures were investigated: 115 K (ICE), 233 K (ICE), 293.6 K (water), and 600 K (water). The objective was to compare the k_{eff}, that is, change in reactivity Δk_{eff} in pcm, where 1 pcm = 0.00001 Δk, between calculations done with both libraries with respect to temperature variation. A cross-cut view of the configuration is provided in Fig. 12. The density of ICE/water corresponding with the different temperatures is provided in Table 6.

The same density value is retained for ICE at 115 K and at 233 K, which seems consistent since the ice density does not change significantly below 233 K (see Fig. 13).

The differences between calculations using JEFF-33_FULL and JEFF-33_SHORT for the OECD/WPNCS/SG3 benchmark are shown in

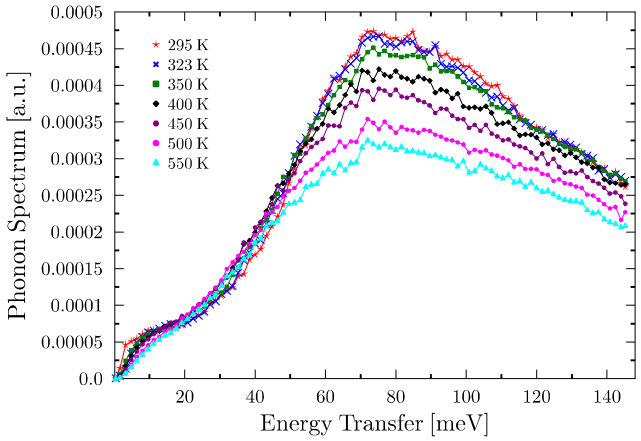

Fig. 11. Phonon spectrum of light water for incident neutron energy E_i= 160 meV.

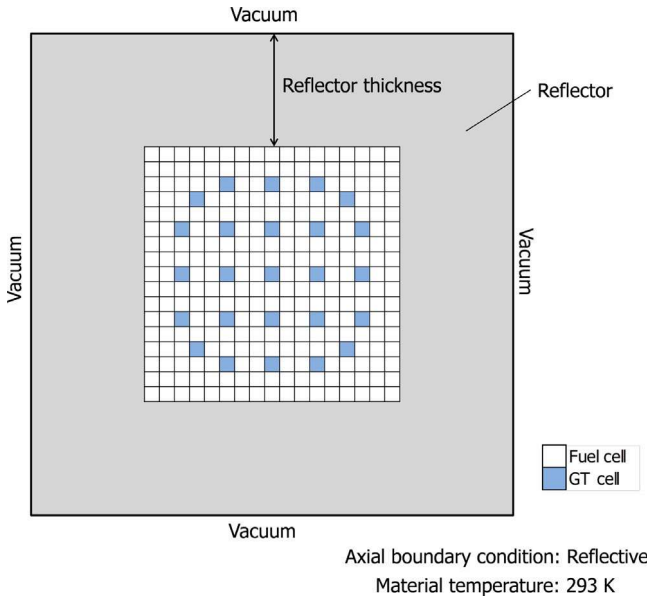

Fig. 12. Cross-cut view of SG3 benchmark assembly.

Table 7
Δk_{eff} temperature differences with 7 PCM standard deviation.

Values	$EALF$ (eV)	JEFF-3.3_FULL–JEFF-3.3_SHORT (PCM)
115 K	0.299	−25
233 K	0.324	−16
293.6 K	0.310	−26
600 K	0.622	−16

Table 7. With a 7 PCM standard deviation the differences in Table 7 are statistically the same.

It can be seen that the results from JEFF-3.3_FULL and JEFF-3.3_SHORT because of the representation of the ^{235}U section lead to a negative change in reactivity with absolute values less than 100 pcm. No clear trend is observed when the temperature increases, even when $EALF$ increases with temperature, meaning that the neutron spectrum shifts to higher energies.

For the second benchmark, the concentration of ^{235}U was set equal to 2.39981×10^{-4} atom/barn. The hydrogen content (in ice or water) was considered variable depending on the moderation ratio, which consists of the number of moderating nuclei (hydrogen) and the number of fuel nuclei (uranium), that is, $N_H/N_{U^{235}}$. The moderation ratio ranged from 2 to 2004. Note that situations with low moderation ratios might exist in

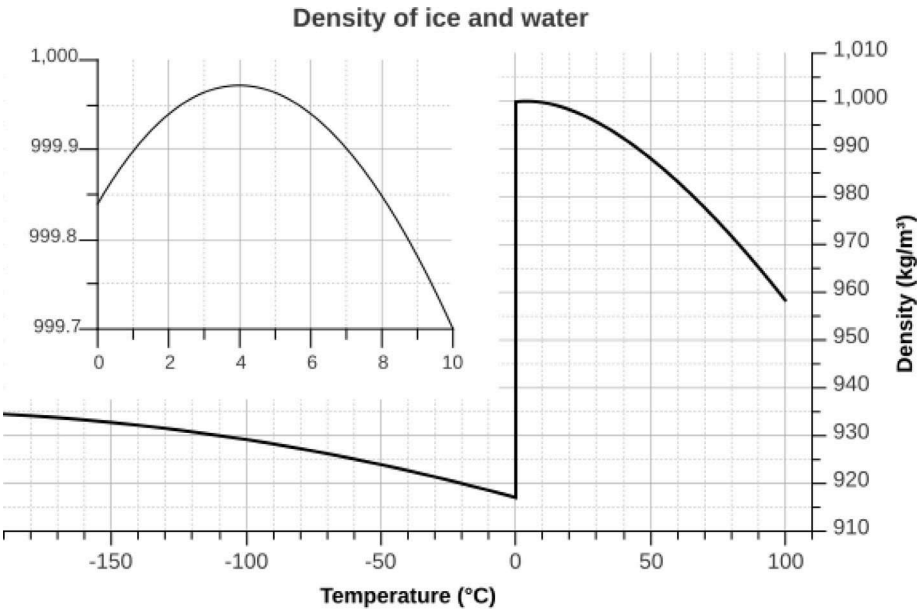

Fig. 13. Density of ice and water versus temperature.

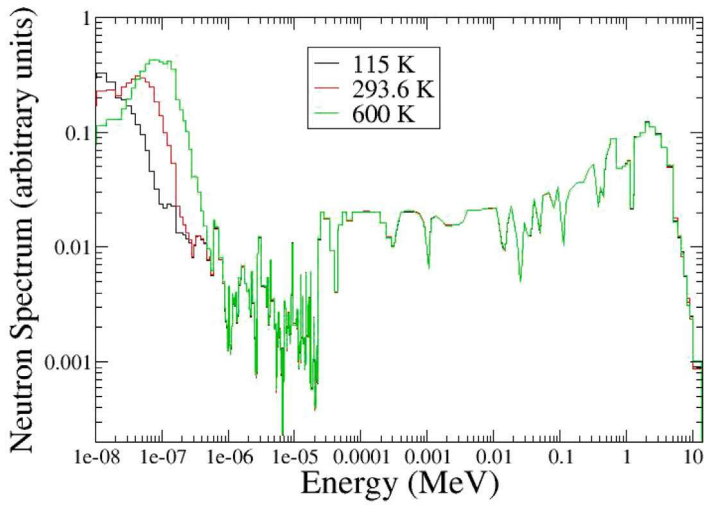

Fig. 14. Neutron fluxes for three temperatures for the moderation ratio of 2010.

criticality safety applications. For benchmark systems representative of thermal reactors, moderation ratios vary from 1000 to 2000 (Bernnat et al., 1986). The neutron spectra in arbitrary units corresponding to a $EALF = 0.0331$ eV at 115 K, 293.6 K and 600 K are displayed in Fig. 14.

The Δk_{eff} differences, in pcm, between JEFF-33_FULL and JEFF-33_SHORT calculations are displayed in Table 8 and Fig. 15.

The Δk_{eff} differences from the FULL and SHORT evaluations of ^{235}U cross sections do not strongly depend on the moderation ratio, even if there is a minimum value at the moderation ratio of 100. A further study consisted of replacing the thermal scattering data of hydrogen in water with other evaluations, for instance that of ENDF/B-VIII.0 and also by the free gas model. The trend on the Δk_{eff} differences from FULL and SHORT remained unchanged.

We also tested the two libraries (SHORT and FULL) for ^{235}U on various benchmarks from the ICSBEP Handbook. The JEFF-3.3 library was used for all other nuclides. The benchmarks are listed as follows.

- ORNL spheres (HEU-SOL-THERM-013) benchmark at room temperature. For this benchmark, the moderation ratio varies between 972 and 1378. The discrepancy observed between k_{eff} is

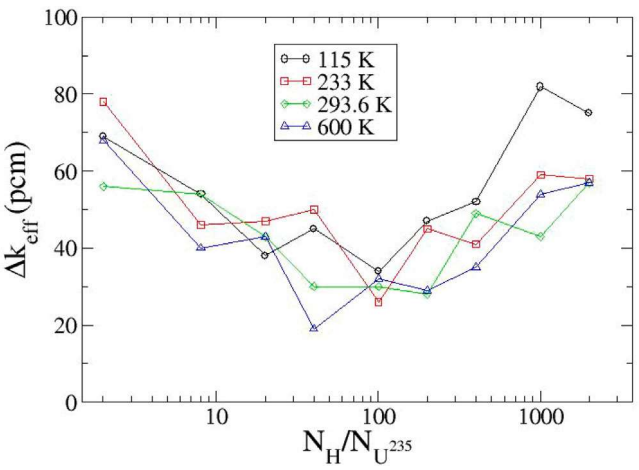

Fig. 15. Differences between JEFF3_FULL and JEFF3_SHORT as a function of temperature and moderation ratio.

Table 8
k_{eff} Difference versus evaluation of ^{235}U and versus temperature.

	JEFF-3.3_FULL–JEFF-3.3_SHORT (ppm)							
	T = 115 K		T = 223 K		T = 293.6 K		T = 600 K	
Moderation Ratio	EALF (eV)	Δk_{eff}	EALF (eV)	Δk_{eff}	EALF (eV)	Δk_{eff}	EALF (eV)	Δk_{eff}
2.004	6970	−69	7060	−78	7110	−56	7210	−68
8.016	111	−54	113	−46	114	−54	117	−40
20.04	8.27	−38	8.41	−47	8.54	−43	9.09	−43
40.08	1.44	−45	1.47	−50	1.51	−30	1.71	−19
100.2	0.222	−34	0.237	−26	0.248	−30	0.326	−32
200.4	0.080	−47	0.092	−45	0.0996	−28	0.150	−29
400.8	0.0398	−52	0.0502	−41	0.0563	−49	0.0936	−35
1002	0.0227	−82	0.0327	−59	0.0381	−43	0.0668	−54
2004	0.0180	−75	0.0279	−58	0.0331	−57	0.0617	−57

Table 9
k_{eff} Difference of k_{eff} between SHORT and FULL cross sections for various benchmarks.

Series	Moderation ratio (eV)	k_{eff}(FULL)	k_{eff}(SHORT)	Difference (FULL–SHORT) (pcm)
HEU-COMP-INTER-004.c01	0.45	1.36000	1.36026	−26
HEU-MET-FAST-001.c01	0	1.00048	1.00054	−6
HEU-SOL-THERM-013.c01	1370	1.00270	1.00273	−13
HEU-SOL-THERM-013.c02	1170	1.00321	1.00317	+4
HEU-SOL-THERM-013.c03	1030	1.00087	1.00134	−47
HEU-SOL-THERM-013.c04	971	1.00325	1.00390	−65
LEU-SOL-THERM-019.c149	728	1.01228	1.01302	−74
HEU-SOL-THERM-004.c06	431	1.05221	1.05254	−33
HEU-SOL-THERM-020.c01	230	1.11106	1.11154	−48
LEU-COMP-THERM-007.c04	NA[a]	1.00440	1.00478	−38
HEU-MET-INTER-006.c01	NA	1.07892	1.07965	−73
HEU-MET-INTER-006.c02	NA	1.06479	1.06538	−59
HEU-MET-INTER-006.c03	NA	1.04472	1.04508	−36
HEU-MET-INTER-006.c04	NA	1.01807	1.01856	−49

[a] NA stands for not applicable since there is no homogeneous solution.

Table 10
Flux distribution (in percent) versus moderation ratio and temperature.

Moderation ratio	115 K			293.6 K			600 K		
	Fast	Epithermal	Thermal	Fast	Epithermal	Thermal	Fast	Epithermal	Thermal
2.01	73.61	26.39	0.00	73.72	26.26	0.00	73.80	26.18	0.00
140.7	49.29	36.18	14.52	48.50	35.71	15.79	46.34	34.17	19.49
1005	34.29	26.66	39.05	30.41	23.58	46.01	25.05	19.45	55.50

less than 65 pcm, which is consistent with the results obtained on the SG3 and fictitious benchmarks.

- Benchmarks involving uranyl fluoride solutions in heavy water reflected or not by heavy water (HEU-SOL-THERM-004 and HEU-SOL-THERM-020).
- A STACY benchmark (LEU-SOL-THERM-019) with slabs of uranyl nitrate solution reflected by polytethylene.
- The GODIVA benchmark (HEU-MET-FAST-001).
- A k_{∞} benchmark (HEU-COMP-INTER-004) in intermediate neutron spectrum.
- A benchmark involving UO_2 rods in water (LEU-COMP-THERM-007).
- A benchmark intermediate spectrum critical assemblies with a graphite HEU core surrounded by a copper reflector (HEU-MET-INTER-006).

The FULL-SHORT differences in Table 9 are quite consistent with the values obtained in 7 and 8.

To better understand the increasing effect of the resonance treatment with the moderation ratio at 600 K, the distribution of the flux versus the energy of neutrons was analyzed for three moderation ratios: 2.01, 140.7, and 1005 (Table 10).

For the 2.01 and 140.7 moderation ratios, when temperature increases, the percentage of the thermal flux of neutrons remains constant. On the contrary, for a moderation ratio of 1005, when temperature increases, the percentage of thermal neutrons increases whereas the percentage of epithermal and fast neutrons decreases. This could be the reason why the k_{eff} discrepancy between the ^{235}U libraries decreases. For ^{235}U the energy range for the resonance region is up to 25 keV. Above this energy is the high energy region. The thermal moderation rate of 2.01 indicates an insignificant fraction of neutrons below 25 keV.

At a given temperature, when the moderation ratio increases, the percentage of fast neutron flux decreases, the percentage of epithermal flux increases, then decreases, and the percentage of thermal flux increases.

The change of temperature in a criticality configuration has two main effects: (1) it leads to a modification of cross sections because of the Doppler effect and (2) it leads to a variation of the density of the material.

To compare the effect of temperature on nuclear data and the effect of temperature on the density, the SG3 benchmark was used to vary the density of water between its value at 293.6 K (0.998 g/cm^3) and the value given for ice at 233 K (0.9228 g/cm^3). The k_{eff} difference corresponding with the decrease of density is −2875 pcm, which is far higher than the effect associated with the missing resonances of ^{235}U cross sections. Consequently, the exact knowledge

of the density at the desired temperature is more important with regard to criticality safety than the reconstruction of the exact number of ^{235}U resonances in the resolved resonance range at that temperature. The SHORT set of resonances can therefore be used in place of the FULL set of resonances at any temperature above 100 K without significantly perturbing the k_{eff} results. The density of the moderator will always remain predominant.

5. Conclusion

An approach has been developed to investigate the impact of temperature effects in practical situations. First, the temperature effects on the differential data, mainly the cross section, were investigated by simulating the cross-section data for an ^{235}U isotope, such as in the resolved resonance region from thermal to 2.25 keV. The ^{235}U cross-section data resembled the actual data since the simulated experimental data were generated based on actual average resonance data. Additionally, experimental effects, for instance resolution, were added to the data. The simulated data were generated based on the reduced Reich–Moore R-matrix formalism. The actual ^{235}U JEFF-3.3 evaluation was used as a template in which the portion corresponding to the resolved resonance was replaced by the simulated resolved resonance parameters. The strategy consisted of generating resonance parameters, by sampling known statistical distributions, including all resonances (full set) with no missing resonances. Further steps consisted of constructing a smaller set of resonances by fitting the simulated cross-section data. The result is a set of resonance parameters containing $\sim$ 40 % less resonances (short set) that, however, fitted well the simulated data generated with the full resonance parameter set. Cross-section libraries in the ENDF format were generated based on the full and short sets, respectively. These libraries were processed by the NJOY code to generate temperature-dependent libraries for testing. An interesting pattern was seen by comparing the cross sections for temperatures from 100 to 900 K. Fig. 8 shows that the cross section generated for the SHORT and FULL sets of resonance parameters are equivalent down to the temperature of 200 K. Below 200 K care must be taken since the differences are noticeable. On the other hand, the higher the temperature, smaller differences are observed, which favors the use of fewer resonances for higher temperatures.

For thermal systems, the effects of temperature are highly noticeable for the thermal scattering of neutrons. TSLs for light water and ice, $S(\alpha, \beta)$, were generated at various temperatures on the basis of the actual frequency spectrum for measurements carried out at SNS. Likewise, thermal scattering libraries in the ENDF format were generated.

The impact of the temperature effects in practical applications was investigated by examining the k_{eff} changes for temperatures below and above room temperature for four temperatures: 115 K, 233 K, 293.6 K, and 600 K. Note that the temperature effects observed in the integral benchmark calculations do not seem to strongly depend on temperature, even if we can observe a decrease for some values of moderation, which is consistent with the tendency highlighted for differential data analysis. Furthermore, integral results indicate that larger differences are observed for higher moderation ratios for which benchmarks are very thermal.

Although the studies and analyzes presented are based on differential data simulations and integral applications and calculations, the results provide interesting insights into whether real data were used. In no way should the results and conclusions presented replace the results of the real experiment.

Declaration of competing interest

The authors declare the following financial interests/personal relationships which may be considered as potential competing interests: Luiz Leal reports financial support was provided by Oak Ridge National Laboratory. Luiz Leal reports a relationship with Oak Ridge National Laboratory that includes: employment. If there are other authors, they declare that they have no known competing financial interests or personal relationships that could have appeared to influence the work reported in this paper.

Data availability

Data will be made available on request.

Acknowledgments

This work was supported by the Nuclear Criticality Safety Program, funded and managed by the National Nuclear Security Administration for the Department of Energy. Part of this work was carried out when the first author, Luiz Leal, was at the Institut de Radioprotection et de Sûreté Nucléaire (IRSN).

References

Herman, M., Trkov, A. (Eds.), 2010. ENDF-6 Formats Manual, Formats and Procedures for the Evaluated Nuclear Data Files ENDF/B-VI and ENDF/B-VII. Report-BNL-90365-2009 Rev. 1, National Nuclear Data Center, Upton, NY.

Bensussan, A., Salome, J.M., 1978. GELINA: a modern accelerator for high resolution neutron time of flight experiments. Nuclear Instrum. Methods 155, 11–23.

Bernnat, Wolfgang, Mattes, Margarete, Arshad, Muhammed, Emendörfer, Dietern, Keinert, Jügen, Pohl, Burkhand, 1986. Ananlysis of Selected Thermal Reactor Benchmark Experiments Based on the JEF-1 Evaluated Nuclear Data File. IKE 6-157, JEF Report 7.

Cabellos, O., Piedra, D., 2018. WPNCS-SG3 benchmark on the effect of temperature on the keff for PWR fuel assemblies: UPM preliminary results, jefdoc-1953.

Carlson, A.D., Pronyaev, V.G., Capote, R., Hale, G.M., Chen, 4.Z.-P., Duran, I., Hambsch, F.-J., Kunieda, S., Mannhart, W., Marcinkevicius, B., Nelson, R.O., Neudecker, D., Noguere, G., Paris, M., Simakov, S.P., Schillebeeckx, P., Smith, D.L., Tao, X., Trkov, A., Wallner, A., Wang, W., 2018. Evaluation of the neutron data standards. Nucl. Data Sheets 148, 143–188.

Cochet, B., Heulers, L., Jinaphanh, A., Jacquet, O., 2015. Capabilities overview of the MORET 5 Monte Carlo code. Ann. Nucl. Energy 74–82.

Gaerttner, E.R., M. L. Yeater, R.R., 1961. Fullwood (1961) rensselaer polytechnic institute linac facility. In: Proceedings of Symposium on Neutron Physics. RPI, May.

Gwin, R., et al., 1984. Measurements of the neutron fission cross sections of ^{235}U (En=0.01 eV to 30 keV) and ^{239}Pu (En=0.01 to 60 eV). Nucl. Sci. Eng. 88, 37. http://dx.doi.org/10.13182/NSE84-A17138.

Harvey, J.A., et al., 1988. High-resolution neutron transmission measurements on ^{235}U,^{239}Pu, and ^{238}U. In: Proc. Int. Conf. Nuclear Data for Science and Technology. Mito, Japan, May 30–June 3.

Hove, L.V., 1954. Correlations in space and time and Born approximation scattering in systems of interacting particles. Phys. Rev. 95 (1), 249–262.

IAEA, 2018, Technical report, IAEA Safety Standards for protecting people and the environment: Regulations for the Safe Transport of Radioactive Material, Specific Safety Requirements, No. SSR-6.

Jaiswal, Vaibhav, Leal, Luiz, Kolesnikov, Alexander I., 2023. Thermal scattering law for ice based on neutron time-of-flight experiments carried out at the SEQUOIA spectrometer at the Oak Ridge National Laboratory. EPJ Web Conf. 284, 17008. http://dx.doi.org/10.1051/epjconf/202328417008.

Larson, N.M., 2008. Updated Users Guide for SAMMY: Multi-Level R-Matrix Fits to Neutron Data using Bayes' Equations. ENDF-364/R2, Oak Ridge National Laboratory, available at the Radiation Safety Information Computational Center (RSICC) as PSR-158.

Leal, L.C., Larson, N.M., 1995. A Computer Code for Calculating Statistical Distribution for R-Matrix Resoancne Parameters. ORNL/TM-13092.

Leal, Luiz, Santos, Adimir Dos, Ivanov, Evgeny, Ivanova, Tatiana, 2017. Impact of ^{235}U resonance parameter evaluation in the reactivity prediction. Nuc. Sci. Eng. 187, 127–141.

Leal, L.C., et al., 1999. R-matrix analysis of ^{235}U neutron transmission and cross-section measurements in the 0- to 2.25-keV energy range. Nucl. Sci. Eng. 131, 230. http://dx.doi.org/10.13182/NSE99-A2031.

MacFarlane, R., 1994. New Thermal Neutron Scattering Files for ENDF/B-VI, Release 2. LA-12639-MS (ENDF-356).

Macfarlane, R., Muir, D., Boicourt, R.M., Kahler, III, A.C., Comstock, A., Conlin, J.L., 2017. The NJOY Nuclear Data Processing System, Version 2016. LA-UR-17-20093.

Marquez Damian, J., Granada, J., Malaspina, D., 2014. CAB models for water: A new evaluation of the thermal neutron scattering laws for light and heavy water in ENDF- 6 format. Ann. Nucl. Energy 65, 280–289.

Mattes, M., Keinert, J., 2005. Thermal Neutron Scattering Data for the Moderator Materials H_2O, D_2O and ZrH_x in ENDF-6 Format and As ACE Library for MCNP(X) Codes. INDC(NDS)-0470, International Nuclear Data Committee.

Otuka, N., Dupont, E., Semkova, V., Pritychenko, B., Blokhin, A.I., Aikawa, M., Babykina, S., Bossant, M., Chen, G., Dunaeva, S., Forrest, R.A., Fukahori, T., Furutachi, N., Ganesan, S., Ge, Z., Gritzay, O.O., Herman, M., Hlavač, S., Katō, K., Lalremruata, B., Lee, Y.O., Makinaga, A., Matsumoto, K., Pikulina, M.G., Pronyaev, V.G., Saxena, A., Schwerer, O., Simakov, S.P., Soppera, N., Suzuki, R., Takács, S., Tao, X., Taova, S., Tárkányi, F., Varlamov, V.V., Wang, J., Yang, S.C., Zerkin, V., Zhuang, Y., 2014. Towards a more complete and accurate Experimental Nuclear Reaction DataLibrary (EXFOR): International collaboration between Nuclear ReactionData Centres (NRDC). Nucl. Data Sheets 120, 272.

Perez, R.B., De Saussure, G., Silver, E.G., 1973. Simultaneous measurements of the neutron fission and capture cross sections for uranium-235 for neutron energies from 8 eV to 10 keV. Nucl. Sci. Eng. 52, 46. http://dx.doi.org/10.13182/NSE73-A23288.

Rubbia, C., et al., 1998. High Resolution Spallation Driven Facility At the CERN-PS To Measure Neutron Cross Sections in the Interval from 1 EV to 250 MeV. CERN/LHC/98-002-EET, Weblink: http://public.web.cern.ch/public/en/research/NTOF-en.html.

Solbrig, A.W., 1961. Doppler effect in neutron absorption resonances. Am. J. Phys. 29, 257, 10.1119/1.1937737.

Spencer, R.R., et al., 1987. Parameters of the 1.056-eV resonance in ^{240}Pu and the 2200 m/s neutron total cross sections of ^{235}U,^{239}Pu, and^{240}Pu. Nucl. Sci. Eng. 96, 318. http://dx.doi.org/10.13182/NSE87-A16395.

The Spallation Neutron Source (SNS), Oak Ridge National Laboratory, Weblink: https://neutrons.ornl.gov/sns.

Weston, L.W., Todd, J.H., 1984. Subthreshold fission cross section of^{240}Pu and the fission cross sections of ^{235}U and^{239}Pu. Nucl. Sci. Eng. 88, 567. http://dx.doi.org/10.13182/NSE84-A18373.